SCIENCE CHINA
Life Sciences

•RESEARCH PAPER•

September 2023 Vol.66 No.9: 2152–2166
https://doi.org/10.1007/s11427-022-2313-1

Functional characterization of novel *NPRL3* mutations identified in three families with focal epilepsy

Shiyue Du[1†], Sheng Zeng[2,3†], Li Song[1†], Hongying Ma[1], Rui Chen[1], Junyu Luo[1], Xu Wang[4], Tingbin Ma[5], Xuan Xu[5], Hao Sun[1,5], Ping Yi[1], Jifeng Guo[2], Yaling Huang[6], Mugen Liu[1], Tao Wang[6], Wei-Ping Liao[7], Luoying Zhang[1,8*], Jing Yu Liu[5*] & Beisha Tang[2,9*]

[1]*Key Laboratory of Molecular Biophysics of Ministry of Education, College of Life Science and Technology, Huazhong University of Science and Technology (HUST), Wuhan 430074, China;*
[2]*Department of Neurology, Xiangya Hospital, Central South University, Changsha 410008, China;*
[3]*Department of Geriatrics, The Second Xiangya Hospital, Central South University, Changsha 410011, China;*
[4]*National Reference Laboratory of Veterinary Drug Residues and MAO Key Laboratory for Detection of Veterinary Drug Residues, Huazhong Agricultural University, Wuhan 430070, China;*
[5]*Institute of Neuroscience, State Key Laboratory of Neuroscience, Center for Excellence in Brain Science and Intelligence Technology, Chinese Academy of Sciences, Shanghai 200031, China;*
[6]*Department of Neurology, Union Hospital of HUST, Wuhan 430022, China;*
[7]*Institute of Neuroscience and Department of Neurology of the Second Affiliated Hospital of Guangzhou Medical University; Key Laboratory of Neurogenetics and Channelopathies of Guangdong Province and the Ministry of Education of China, Guangzhou Medical University, Guangzhou 510260, China;*
[8]*Hubei Province Key Laboratory of Oral and Maxillofacial Development and Regeneration, Wuhan 430022, China;*
[9]*Key Laboratory of Hunan Province in Neurodegenerative Disorders, Central South University, Changsha 410008, China*

Received January 18, 2023; accepted March 1, 2023; published online April 12, 2023

Focal epilepsy accounts for 60% of all forms of epilepsy, but the pathogenic mechanism is not well understood. In this study, three novel mutations in *NPRL3* (*nitrogen permease regulator-like 3*), c.937_945del, c.1514dupC and 6,706-bp genomic DNA (gDNA) deletion, were identified in three families with focal epilepsy by linkage analysis, whole exome sequencing (WES) and Sanger sequencing. NPRL3 protein is a component of the GATOR1 complex, a major inhibitor of mTOR signaling. These mutations led to truncation of the NPRL3 protein and hampered the binding between NPRL3 and DEPDC5, which is another component of the GATOR1 complex. Consequently, the mutant proteins enhanced mTOR signaling in cultured cells, possibly due to impaired inhibition of mTORC1 by GATOR1. Knockdown of *nprl3* in *Drosophila* resulted in epilepsy-like behavior and abnormal synaptic development. Taken together, these findings expand the genotypic spectrum of *NPRL3*-associated focal epilepsy and provide further insight into how *NPRL3* mutations lead to epilepsy.

focal epilepsy, NPRL3, GATOR1, mTOR, abnormal synaptic development

Citation: Du, S., Zeng, S., Song, L., Ma, H., Chen, R., Luo, J., Wang, X., Ma, T., Xu, X., Sun, H., et al. (2023). Functional characterization of novel *NPRL3* mutations identified in three families with focal epilepsy. Sci China Life Sci 66, 2152–2166. https://doi.org/10.1007/s11427-022-2313-1

†Contributed equally to this work
*Corresponding authors (Luoying Zhang, email: zhangluoying@hust.edu.cn; Jing Yu Liu, email: liujy@ion.ac.cn; Beisha Tang, email: bstang7398@163.com)

INTRODUCTION

Focal epilepsy accounts for 60% of all forms of epilepsy, with seizures originating from a specific location in the brain (Devinsky et al., 2018; Perucca, 2018). Familial focal epilepsies mainly display Mendelian inheritance and are characterized by epileptic seizures, such as autosomal dominant nocturnal frontal lobe epilepsy (ADNFE), familial focal epilepsy with variable foci (FFEVF), and familial mesial temporal lobe epilepsy (FMTLE) (Crompton et al., 2010; Riney et al., 2022; Scheffer et al., 1995; Scheffer et al., 1998). These disorders display genetic heterogeneity and involve mutations of genes encoding ion channel subunits (*SCN1A*, *KCNA2*, *CACNA1A*), neurotransmitter receptors (*GABRA1*, *CHRNA4*, *GRIN2A*), synaptic secreted proteins (*LGI1*), cell adhesion proteins (*PCDH19*) and a number of genes in the mechanistic target of rapamycin (mTOR) pathway (*DEPDC5*, *NPRL2*, *NPRL3*) (Myers and Mefford, 2015; Riney et al., 2022; Wang et al., 2017).

The mTORC1 pathway plays a central role in regulating responses to environmental factors such as nutrients and growth factors (Bar-Peled et al., 2013; Saxton and Sabatini, 2017). The GATOR1 protein complex consists of NPRL3, DEPDC5 (DEP domain-containing protein 5), and NPRL2 (nitrogen permease regulator-like 2) and exerts an inhibitory effect on the mTORC1 pathway (Bar-Peled et al., 2013). Since 2013, an increasing number of mutations in GATOR1 leading to a wide range of phenotypes associated with varying disease severity have been reported in individuals with epilepsy (Baldassari et al., 2019; Canavati et al., 2019; Dibbens et al., 2013). Most *NPRL3* mutations lead to nonsense-mediated mRNA decay or loss of function (Dawson et al., 2020; Sim et al., 2016; Weckhuysen et al., 2016). Moreover, phospho-S6 immunostaining in resected brain tissue from patients with *NPRL3* mutations indicated mTORC1 hyperactivity in neurons (Sim et al., 2016; Weckhuysen et al., 2016). However, how these mutations result in activation of the mTOR pathway and downstream signaling events triggered by mTOR activation are still unknown.

Here, we report on three families with focal epilepsy and identify three novel heterozygous germline mutations in the *NPRL3* gene through linkage analysis, whole exome sequencing (WES) and Sanger sequencing. To elucidate the detailed pathogenic mechanism, we examined the effects of these mutations on protein expression, stability, GATOR1 formation and the activation status of downstream targets of the mTOR pathway. Knocking down *nprl3* in fruit flies leads to epilepsy-like behavior and morphological defects of synapses, recapitulating the phenotypes in human patients. In summary, our study provides further understanding of the pathogenic mechanism underlying focal epilepsy.

RESULTS

Clinical features of families with focal epilepsy

Family 1 is a five-generation family with 50 members, including 11 patients (Figure 1A). The median age of first seizure occurrence was 10 (3–50), and the average age was 15.8±14.9. Four patients (III:6, III:12, IV:13 and V:6) displayed abdominal or emotional aura, three patients (III:12, IV:13 and V:6) exhibited focal nonmotor seizures, and the other patients had generalized tonic-clonic seizures (GTCSs) which may or may not be secondary to focal seizures (Table S1 in Supporting Information). All members had normal developmental milestones except one member who displayed intellectual disability (V:6). Most affected individuals exhibited a tendency of clinical remission or termination with age without medication. Brain magnetic resonance imaging (MRI) of the patients (III:12, IV:11, IV:13 and V:6) displayed no obvious abnormality, but interictal electroencephalography (EEG) recorded focal epileptiform discharges with different origins in IV:13 and V:6 (Figure S1A, B and Table S1 in Supporting Information). All the clinical features above indicate that these individuals are likely affected by FFEVF. Detailed clinical information of this family is summarized in Table S1 in Supporting Information.

Family 2 is a five-generation pedigree with autosomal dominant inheritance, including eleven affected individuals, among which nine were alive (Figure 1B). The mean age at seizure onset was 9.2±5.2, ranging from 16 months to 15 years old. Seizure semiology indicated a focal onset in two patients (III:4 and IV:4), while the other seven patients exhibited GTCS, which may or may not be secondary to the focal seizure (Table S2 in Supporting Information). Brain MRI showed no abnormality in the proband (IV:6) (Figure S1C in Supporting Information). Sphenoid electrode with hyperventilation (HV) EEG showed evoked sharp and slow wave complexes from bilateral frontal and temporal lobes (Figure S1D in Supporting Information). The clinical features above also indicated the possibility of FFEVF. Detailed clinical information on family 2 is summarized in Table S2 in Supporting Information.

Family 3 included three members, with the proband (II:1) and his mother (I:2) both diagnosed with nocturnal frontal lobe epilepsy (Figure 1C). The proband had his first seizure at the age of 2 and exhibited behavior arrest and impaired awareness, which lasted for one minute. Video electroencephalography (VEEG) revealed epileptic discharges in his left temporal area during sleep, and MRI showed a possible arachnoid cyst in the anterior longitudinal fissure pool of the brain. His mother also had a history of seizures, and the attacks were self-controlled with age in the absence of treatment.

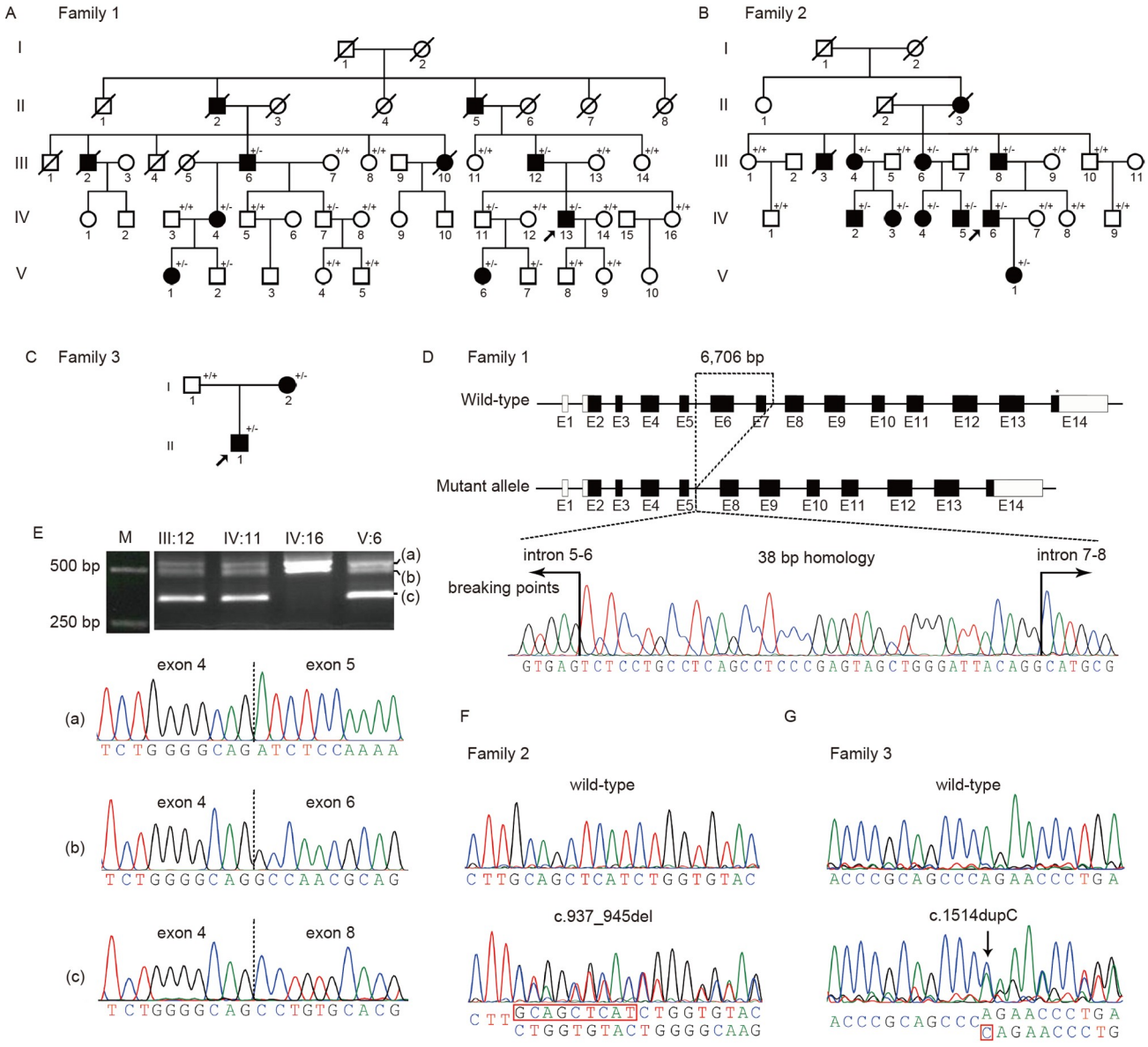

Figure 1 Identification of mutations in the *NPRL3* gene in three pedigrees with focal epilepsy. A–C, The pedigrees of three families with focal epilepsy. The affected individuals are marked by black solid symbols, and an arrow depicts the proband. The wild-type allele is marked as "+", the mutant allele is marked as "-", and "+/-" represents a heterozygous mutation carrier in each family. D, Top panel: Analysis of the microdeletion using genomic DNA as the template in family 1. The picture above is the schematic diagram showing all exons and UTRs of *NPRL3* based on gene model GenBank: NM_001077350.3, and the 6,706-bp deletion is indicated with a dashed box. Bottom panel: Sanger sequencing diagram demonstrating the breakpoints of the microdeletion in *NPRL3*, and the 38-bp sequence between the two arrows indicates the possible location of upstream and downstream breakpoints. E, Gel electrophoresis analysis of *NPRL3* cDNA from PBLs of patients in the families (III:12, IV:11 and V:6) and one normal control (IV:16). Bottom panel: Sanger sequencing of *NPRL3* gene products amplified from the cDNA of PBLs. F, Sanger sequencing confirmation of the identified *NPRL3* mutation in family 2. The red box represents the deleted 9-bp in *NPRL3* c.937_945del. G, Sanger sequencing confirmation of the identified *NPRL3* mutation in individuals of family 3. Vertical arrows indicate the mutation sites.

Genetic analysis identified novel mutations in *NPRL3*

In family 1, linkage analysis and haplotype analysis indicated that the linked region of this family was within approximately 3 Mb spanning *D16S3399* and *D16S3070* on chromosome 16p13.3 (Figure S2A, B and Table S3 in Supporting Information). Further WES revealed no pathogenic or potential pathogenic mutations at the linkage locus. Then, a read depth-based copy number variation (CNV) estimation method was used to reanalyze the WES data and discovered a possible heterozygous microdeletion in the *NPRL3* gene. Sanger sequencing identified the heterozygous 6,706-bp deletion at 16p13.3 NC_000016.10:g.(110143_110181)_(116848_116886)del (Figure 1D; Figure S2C in Supporting Information). Interestingly, we found that there was an identical sequence of 38-bp at the upstream and downstream breakpoints that localized to Alu elements (Figure 1D), indicating that the breakpoints exhibited microhomology, which may explain

the occurrence of large deletions in this region.

Family segregation analysis by real-time quantitative polymerase chain reaction (RT-qPCR) and Sanger sequencing of the genomic DNA revealed that the microdeletion co-segregated with the phenotype, and the mutation was confirmed in six affected individuals and four asymptomatic carriers (IV:7, IV:11, V:2 and V:7) (Figure S2D in Supporting Information). cDNA cloning of peripheral blood lymphocytes (PBLs) from both the patients and normal controls identified two wild-type (WT) *NPRL3* transcripts, a and b (Figure 1E), of which the difference lies in the alternative splicing of exon 5. On the other hand, the patients had an abnormal transcript c that lacked exons 5, 6 and 7 (c.319_629del/p.Ile107Profs*56) (Figure 1E), implicating an abnormal splicing event of *NPRL3* mRNA in the patients.

In family 2, WES of III:4 and IV:6 was conducted, and mutations in coding regions, exon-intron boundaries, untranslated regions, and flanking regions (±1,000 bp) were filtered. Among these mutations, 21 candidate genes were screened based on gene function and anatomical expression (Table S4 in Supporting Information). In the end, 19 candidate mutations were excluded by Sanger sequencing and co-segregation analysis. Both *NPRL3* c.937_945del/p.Ala313_His315del and *NARFL* c.461C>T/p.Thr154Ile co-segregated with the disease (Figure 1B and F; Figure S3 in Supporting Information). The *NARFL* c.461C>T/p.Thr154Ile was later excluded, as *NARFL* mutation has been reported in autosomal recessive diffuse pulmonary arteriovenous malformations (Liu et al., 2017). The *NPRL3* c.937_945del/p.Ala313_His315del was absent in 100 unrelated healthy controls by restriction fragment length polymorphism (RFLP) analysis. In addition, the deletion was rated "deleterious" with a score of −22.354 in PROVEAN. Taken together, the *NPRL3* c.937_945del/p.Ala313_His315del was considered to be the causative mutation in this family.

In family 3, the WES data of the three family members were screened, and a novel mutation c.1514dupC in *NPRL3* was identified and verified by Sanger sequencing (Figure 1G). The insertion of a single cytosine at nucleotide position 1,514 altered the translation frame, generating a premature translation termination codon (TGA), and was predicted to produce a truncated protein (p.Gln505Profs*4).

These mutations in *NPRL3* were not present in the Genome Aggregation Database (gnomAD), the Exome Aggregation Consortium (ExAC) or the 1000 Genomes Project.

Effects of *NPRL3* mutations on gene expression

To explore whether these mutations lead to mRNA decay, the secondary structure of *NPRL3* mRNA was predicted using the free energy minimization method. The secondary structure and the minimum free energies (MFE) of c.319_629del-*NPRL3* mRNA were altered substantially compared with WT mRNA, while c.937_945del- and c.1514dupC-*NPRL3* mRNA did not show large differences compared with WT (Figure S4A–H in Supporting Information). The levels of mutant *NPRL3* mRNAs did not change significantly in transfected HEK293 cells compared with WT cells (Figure S4I in Supporting Information). These results indicate that the expression levels of mutant *NPRL3* mRNAs are not affected.

To assess the protein levels of *NPRL3* mutants, we transfected HEK293 cells with WT and mutant NPRL3 plasmids. Western blot analysis showed that the truncated p.Gln505Profs*4 and p.Ile107Profs*56 proteins displayed increased levels compared with WT, while the expression level of p.Ala313_His315del was similar to WT (Figure 2A–C). Next, we assessed the degradation rate of these NPRL3 mutants by cycloheximide (CHX) treatment, which inhibits protein synthesis, and found that the degradation rate of p.Ile107Profs*56 increased, while NPRL3 p.Gln505Profs*4 and p.Ala313_His315del showed a decreased degradation rate (Figure 2D and E). To test whether the differences in the rate of degradation were caused by abnormal localization, we performed immunofluorescence experiments and found that both WT and mutant NPRL3 were mainly localized in the cytoplasm of HEK293 cells (Figures 2F and 3A).

NPRL3 mutations impair the interaction with DEPDC5

Since NPRL3 is a component of the GATOR1 protein complex (Bar-Peled et al., 2013), we investigated whether these *NPRL3* mutations disrupted the formation of the GATOR1 complex. Three-dimensional structures of WT and mutant NPRL3 proteins were predicted by SWISS-MODEL based on the crystal structure of the GATOR1 complex. p.Ala313_His315del mutation led to loss of amino acids Ala313-Ala314-His315 located in a β-sheet of the INT domain, but the overall structure of NPRL3 p.Ala313_His315del showed no significant change compared with NPRL3-WT (Figure S5A and B in Supporting Information). The frameshift mutation NPRL3 p.Gln505Profs*4 lacked part of the C-terminal domain and p.Ile107Profs*56 lost most of the structure and retained only a part of the Longin domain (Figure S5C and D in Supporting Information). These data suggest that the changes in protein structure may affect the function of NPRL3 in the GATOR1 complex. Furthermore, the predicted structure of the GATOR1 complex showed that WT NPRL3 contacted NPRL2, while mutant NPRL3 lost most of its contact with NPRL2 (Figure S5E–H in Supporting Information).

NPRL3 is known to dimerize with NPRL2 and integrates DEPDC5 to form the GATOR1 complex (Bar-Peled et al., 2013; Neklesa and Davis, 2009). Next, we tested whether *NPRL3* mutations impaired the interaction between NPRL3

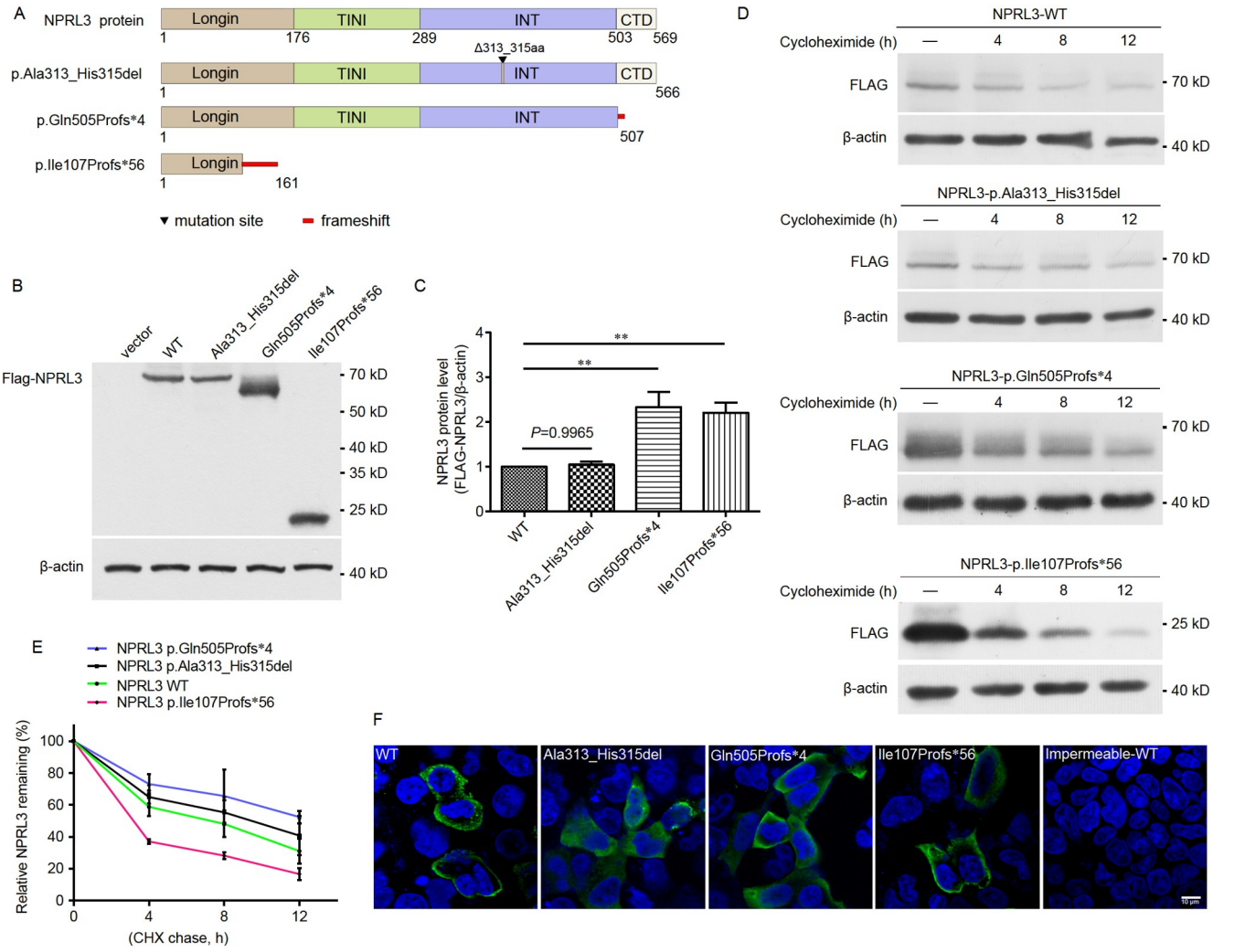

Figure 2 *NPRL3* mutations differentially altered protein expression levels and protein stability. A, Schematic structure of the WT and mutant NPRL3 proteins. The colored boxes represent the domains of NPRL3. B, Representative Western blots of WT and mutant NPRL3 protein in HEK293T cells. C, Quantification of FLAG-NPRL3/β-actin in the Western blot, which was normalized to the value obtained for FLAG-NPRL3-WT. The data are presented as the mean±S.E.M. using one-way ANOVA with Dunnett's multiple comparisons test. **, $P<0.01$. $n=4$. D, Representative Western blots of NPRL3 in HEK293T cells expressing WT NPRL3 or the mutants and treated with 30 μg mL^{-1} CHX for different lengths of time (0, 4, 8 and 12 h). E, Statistical analysis of (D) and the degradation rate of mutant NPRL3 showed no significant difference compared with WT NPRL3. Statistical significance was calculated using one-way ANOVA with Dunnett's multiple comparisons test. $n=3$. F, Representative confocal images showing the subcellular localization of WT and mutant NPRL3 in HEK293 cells. The cells were immunostained with a mouse anti-FLAG antibody (green). Impermeable WT was used as a control, and the cells were not treated with Triton X-100. Scale bar, 10 μm.

and NPRL2. We first assessed the subcellular localization of NPRL3 and NPRL2 in HEK293 cells. Immunofluorescence confirmed the colocalization of the three NPRL3 mutants with WT NPRL2, distributed in discrete punctate structures (Figure 3A). Further co-immunoprecipitation (co-IP) experiments demonstrated that all of the NPRL3 mutants interacted with NPRL2 and showed no significant difference relative to NPRL3-WT (Figure S6 in Supporting Information). These results demonstrate that the truncated NPRL3 protein is still able to dimerize with NPRL2, suggesting that the residual NPRL3 sequences are sufficient for binding to NPRL2.

To exclude potential interfering interactions among the different domains, we constructed five plasmids expressing various forms of truncated NPRL3 proteins and found that all five truncated NPRL3 proteins could bind to full-length NPRL2 (Figure 3B and C), suggesting that NPRL3 and NPRL2 interact via multiple domains. Therefore, we directly introduced the deletion of Ala313_His315 to the NPRL3-INT domain and analyzed the impact of p.Ala313_His315del on the interaction between the NPRL3-INT domain and NPRL2. The results showed that p.Ala313_His315del did not affect the interaction between the NPRL3-INT domain and NPRL2 (Figure 3D and E).

Interestingly, co-IP experiments demonstrated that the mutations severely hampered the interaction between NPRL3 and endogenous DEPDC5 (Figure 3F). We next measured the level of endogenous DEPDC5 protein in HEK293 cells transfected with mutant *NPRL3* and found that

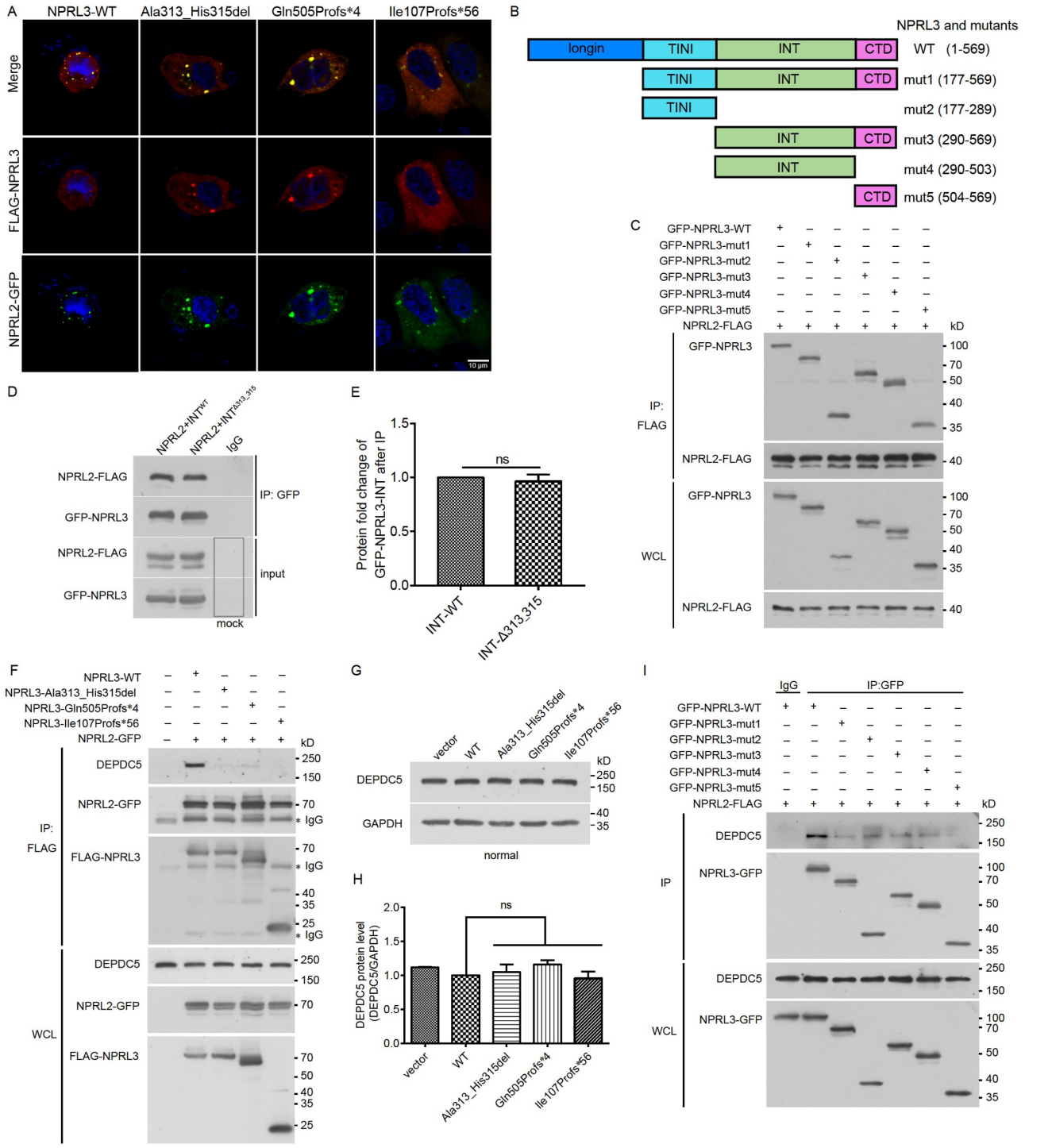

Figure 3 *NPRL3* mutations disrupted the interaction with DEPDC5 but not NPRL2. A, Representative confocal images showing the colocalization of NPRL3 and NPRL2. HEK293 cells were co-transfected with FLAG-NPRL3 (red) and NPRL2-GFP (green). WT-NPRL3 and NPRL2 colocalized in HEK293 cells. The p.Ala313_His315del, p.Gln505Profs*4 and p.Ile107Profs*56 mutants also colocalized with NPRL2. DAPI, 4,6-diamidino-2-phenylindole. Scale bar, 10 μm. B, Schematic model of WT NPRL3 and five NPRL3 truncation mutants. Blue represents the Longin domain, and light blue represents the TINI domain. Green represents the INT domain, and red represents the CTD domain. C, Assessment of interactions between full-length NPRL2-FLAG and different domains of GFP-NPRL3 by co-IP in HEK293T cells. *n*=3. D, The *NPRL3* p.Ala313_His315del mutation did not affect the interaction between the INT domain and full-length NPRL2. E, Quantification of NPRL3-INT-Δ313_315/NPRL2 in the Western blots, which was normalized to the value obtained for INT-WT. The data are represented as the mean±S.E.M. using unpaired *t*-test. F, Assessment of interactions between mutant FLAG-NPRL3 and DEPDC5 by co-IP assays in HEK293T cells. *n*=3. G, *NPRL3* mutations did not affect the protein expression level of DEPDC5. Representative Western blots of DEPDC5 in HEK293 cells transfected with WT or mutant NPRL3 under normal culture conditions. *n*=3. H, Quantification of the DEPDC5/GAPDH ratio in (G). One-way ANOVA with Dunnett's multiple comparisons test. *n*=3. I, Assessment of interactions between truncation mutants of NPRL3-GFP and DEPDC5 by co-IP assays in HEK293T cells. HEK293T cells were co-transfected with NPRL3-GFP (WT or mutants) and FLAG-NPRL2. WCL stands for whole cell lysates.

the mutations did not affect DEPDC5 expression (Figure 3G and H). To further probe the mechanism underlying the interaction between NPRL3 and DEPDC5, we carried out co-IP experiments and found that all truncated domains of NPRL3 (mut 1–5) were able to interact with DEPDC5, but the binding affinity was reduced compared with that of WT NPRL3 (Figure 3I).

Taken together, these results suggested that the three mutations perturbed the interactive interface and impaired the formation of the GATOR1 complex.

NPRL3 mutations enhanced the activation of the mTOR signaling pathway

Mutations in *NPRL3* have been reported to enhance the activation level of the mTORC1 signaling pathway and lead to increased phosphorylation of S6 ribosomal protein (pS6) (Sim et al., 2016). To assess the functional impact of the three *NPRL3* mutations on the mTOR pathway, we measured the phosphorylation of p70 S6 kinase (p70S6K) and pS6. In fresh medium, none of the *NPRL3* mutants significantly affected p70S6K or pS6 (Figure 4A and B; Figure S7A–E in Supporting Information). However, after 1 h of amino acid deprivation, the pS6/S6 ratio showed varying degrees of increase in cells expressing mutant NPRL3 when compared with cells expressing WT NPRL3 (Figure 4C and D).

Leucine, an mTOR agonist, signals to mTORC1 through the well-studied Rag GTPase signaling pathway via Sestrin2/SAR1B-GATOR2-GATOR1 (Chen et al., 2021; Wolfson et al., 2016). We depleted all amino acids in the culture medium and replenished it with L-leucine. We found that leucine activated mTORC1 in a dose-dependent manner, as the mTOR pathway was significantly activated after 10 min of leucine stimulation (Figure S7F and G in Supporting Information). To further examine the effects of the *NPRL3* mutations on the mTORC1 pathway, we measured pS6/S6 ratios after leucine treatment. The results showed that the pS6/S6 ratio of cells transfected with mutant NPRL3 was significantly higher than that of cells transfected with WT NPRL3 (Figure 4E and F). In addition, we assessed DEPDC5 levels in leucine-treated cells and observed no significant differences between the mutants and WT (Figure S7H and I in Supporting Information), indicating that the effects of mutant NRPL3 on mTOR signaling are not caused by a reduction in DEPDC5 levels.

Taken together, these data demonstrated that *NPRL3* mutations enhanced the activation level of the mTOR pathway, likely by impairing the inhibitory function of GATOR1 on mTORC1 signaling.

Deficiency of GATOR1 components led to epileptic-like behavior in flies

Since the *NPRL3* mutations we identified here appeared to impair the function of GATOR1, we next tested whether deficiency of GATOR1 components led to epileptic behavior *in vivo*. *Drosophila nprl3* shared 39.57% amino acid sequence identity with the human *NPRL3* ortholog (Figure S8 in supporting information). We first knocked down *nprl3* in all cells in the fly body using a *tubulin* (*tub*) GAL4 to drive the expression of two different RNAi lines (Fridell et al., 2005), and the knockdown (KD) efficiency was validated by RT-qPCR (Figure S9A and B in Supporting Information). We employed the bang-sensitive seizure (BSS) assay to assess epileptic-like behaviors in flies. Compared with the controls, significantly larger portions of RNAi flies showed seizure/paralysis-like behavior after a vortex "bang" (Figure 5A–D; Movies S1 and S2 in Supporting Information), suggesting that reducing *nprl3* expression increases epileptic-like behavior. The flies that experienced seizure/paralysis needed several minutes to recover (Figure 5E and F), further implying the severity of the epileptic-like behavior. We also employed a weaker ubiquitous driver, *actin*GAL4 (Ji and Clark, 2006), to knock down *nprl3* and then conducted a BSS test (Table S5 in Supporting Information). This resulted in a small but significant increase in seizure/paralysis-like behavior. To test whether there is an age-dependent effect on epilepsy-like behavior, we conducted BSS assays on flies 3, 10 and 30 days after eclosion. A significantly higher ratio of RNAi flies 10 and 30 days post-eclosion displayed seizure/paralysis-like behavior compared with flies 3 days post-eclosion, while there was no significant difference in this ratio between flies 10 *vs*. 30 days post-eclosion (Figure S10A in Supporting Information). However, the recovery time was prolonged in flies 30 days post-eclosion compared with those 10 days post-eclosion (Figure S10B in Supporting Information). As components of the GATOR1 complex, many mutations in *NPRL2* and *DEPDC5* have also been identified in patients with epilepsy (Baldassari et al., 2019). Therefore, we knocked down *nprl2* and *iml1* (the *Drosophila* ortholog of human *DEPDC5*) in all cells and conducted BSS assays (Figure S11 in Supporting Information). A significant increase in the portion of flies that exhibited seizure/paralysis-like behavior was also observed. Taken together, these results indicate that lack of *nprl3* or any one of the other two GATOR1 components enhances epilepsy-like behaviors.

Knockdown of *nprl3* led to abnormal synaptic morphology at the fly neuromuscular junction

NPRL3 mutation carriers started to experience epilepsy in their childhood or teens, implying developmental problems caused by *NPRL3* deficiency (Wullschleger et al., 2006). Therefore, we assessed whether the *nprl3* RNAi flies also displayed developmental defects. Larval NMJs are a well-established system for studying synaptic morphology and function in flies (Keshishian et al., 1996; Menon et al., 2013).

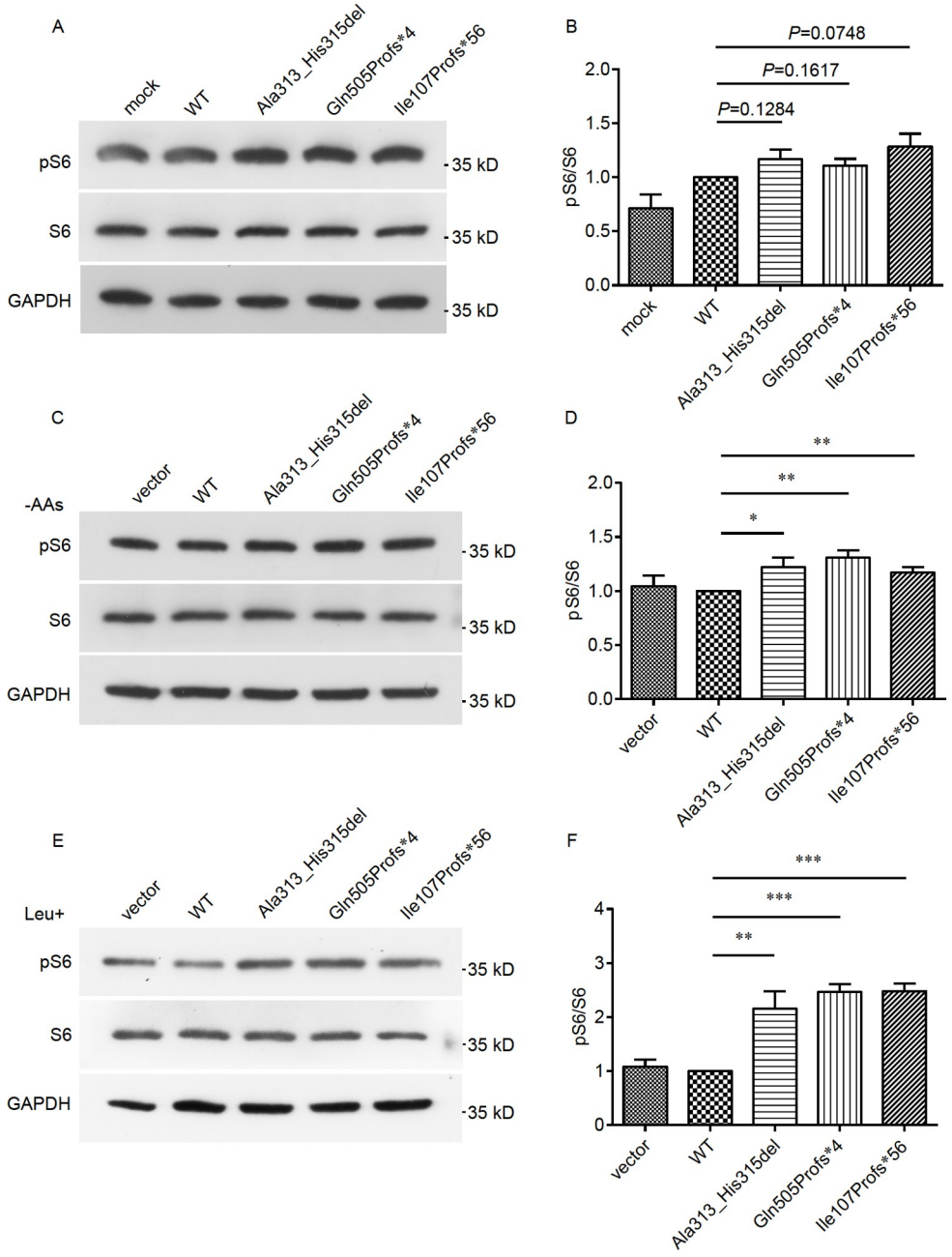

Figure 4 *NPRL3* mutations enhanced the activation level of the mTORC1 signaling pathway. A, Representative Western blots of pS6 in HEK293 cells transfected with WT or mutant FLAG-NPRL3. Mock represents cells without any treatment, which were used as the negative control. B, Quantification of the pS6 (S240/244) to S6 ratio in (A). Data are represented as the mean±S.E.M. using an unpaired *t*-test. n=3. C, Representative Western blots of pS6 in transfected HEK293 cells that were deprived of amino acids for 1 h. The cells were transfected with p3×FLAG vector, WT or the indicated mutants. Vector was used as the negative control. D, Quantification of the pS6 (S240/244) to S6 ratio in (C). Data are represented as the mean±S.E.M. using an unpaired *t*-test. *, P<0.05; **, P<0.01. n=5. E, Representative Western blots of pS6 in transfected HEK293 cells treated with 100 mmol L^{-1} L-leucine after amino acid starvation, and cell lysates were analyzed by Western blotting using the indicated antibodies. Leu, L-leucine. F, Quantification of the pS6 (S240/244) to S6 ratio in (E). Data are represented as the mean±S.E.M. using one-way ANOVA with Dunnett's multiple comparisons test. **, P<0.01; ***, P<0.001. n=4.

We found that the number of type I synaptic boutons in the RNAi flies was increased significantly compared with that in the controls (Figure 6A and B). Type I boutons are known to release synaptic vesicles containing mostly glutamate, and glutamate receptors have been reported to be expressed at these synapses (Schmid et al., 2008). We tried to examine glutamate receptor expression in the brain by immunofluorescence but failed. However, Western blotting revealed elevated glutamate receptor protein levels in the RNAi flies (Figure 6C and D), consistent with an increase in type I boutons.

To investigate whether lack of *nprl3* during development (before eclosion) or in adults is sufficient for epilepsy-like behavior, we adopted a temperature-sensitive *tub*GAL80^{ts}

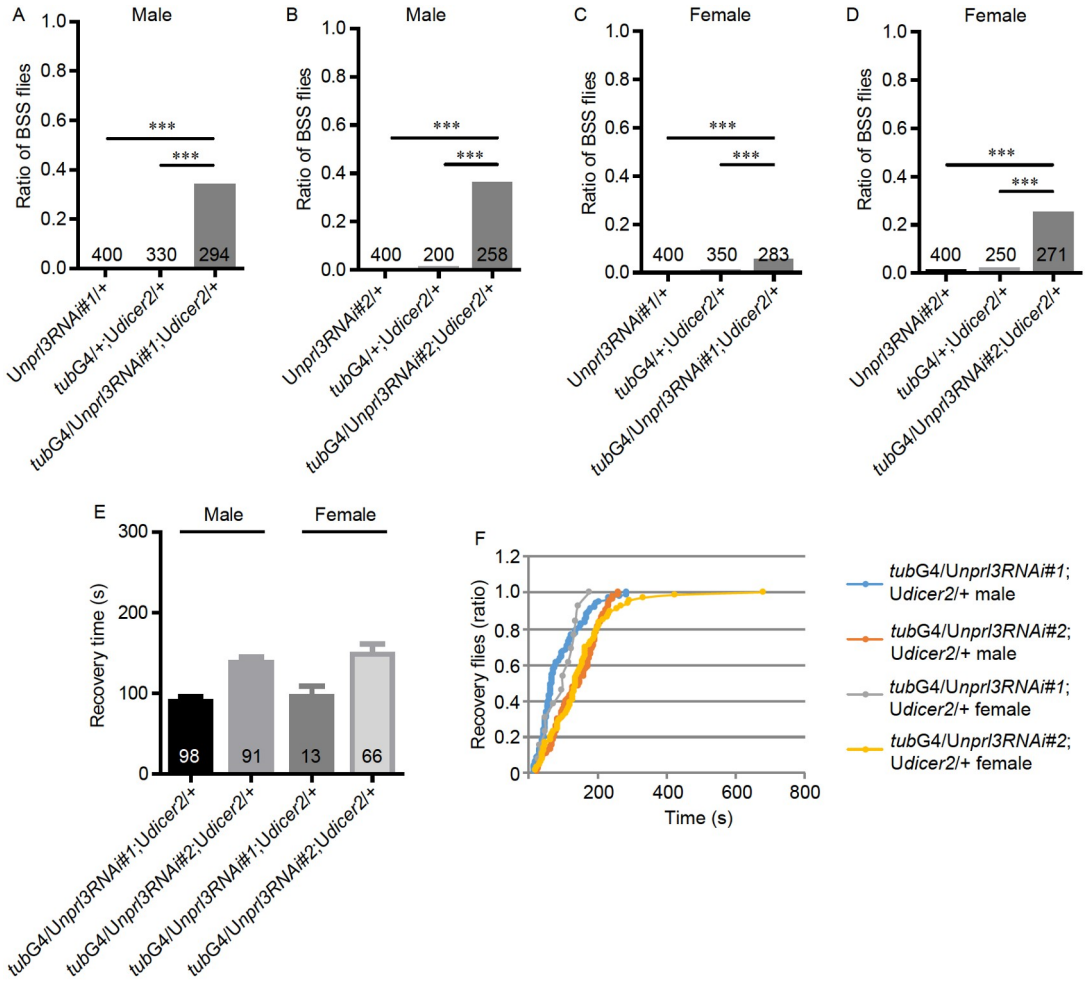

Figure 5 Knocking down *nprl3* led to epilepsy-like behaviors in adult flies. A–D, *nprl3* was knocked down by crossing *tub*GAL4 with two different *nprl3* RNAi lines, 1 (A and C) and 2 (B and D). Ten-day-old flies were used. Statistical differences were calculated by the chi-square test. ***, $P<0.001$. The number of flies used is indicated on the bar. E, The average paralytic recovery time of *nprl3* RNAi flies. F, The ratio of recovered flies at different times post bang. Each dot represents a single fly. G4, GAL4. U, UAS. The data are presented as the mean±S.E.M.

system (McGuire et al., 2004). At the permissive temperature (18°C), GAL80^{ts} is expressed in all cells, repressing GAL4 activity and thus RNAi expression. At the restrictive temperature (29°C), on the other hand, GAL80^{ts} was inactivated, allowing the expression of RNAi. Knocking down *nprl3* specifically during development resulted in lethality, and thus we failed to obtain adult flies for behavior analysis, while knocking down *nprl3* specifically during the adult stage did not lead to increased epilepsy-like behavior (Figure 6E).

In summary, these results indicated that a lack of *nprl3* affected the development of the nervous system, which may contribute to epilepsy-like behavior.

DISCUSSION

In this study, we report on three families with focal epilepsy and identified three novel mutations in *NPRL3*, including c.937_945del, c.1514dupC and a 6,706-bp gDNA deletion. To date, 23 germline mutations (including three mutations in this study) have been identified in the *NPRL3* gene as being linked to epilepsy (Figure S12 in Supporting Information) (Baldassari et al., 2019; Canavati et al., 2019; Korenke et al., 2016; Li et al., 2021; Ricos et al., 2016; Sim et al., 2016; Weckhuysen et al., 2016). Clinical features of the three families exhibited high heterogeneity, ranging from slight eye blinking to severe GTCS, and individuals III:8 and IV:6 of family 2 exhibited symptoms of cyanosis (Tables S1 and S2 in Supporting Information). The severity of epilepsy phenotypes correlates with altered protein function or dosage (Kingdom and Wright, 2022; Liu et al., 2022; Tang et al., 2020). It has been reported that *NPRL3* mutations can lead to variable degrees of epilepsy phenotypes, ranging from asymptomatic to severe developmental delay. Variable penetrance has also been observed in families with other GATOR1 variants (Baldassari et al., 2019). Thus, we suspect that the phenotype severity potentially depends on the se-

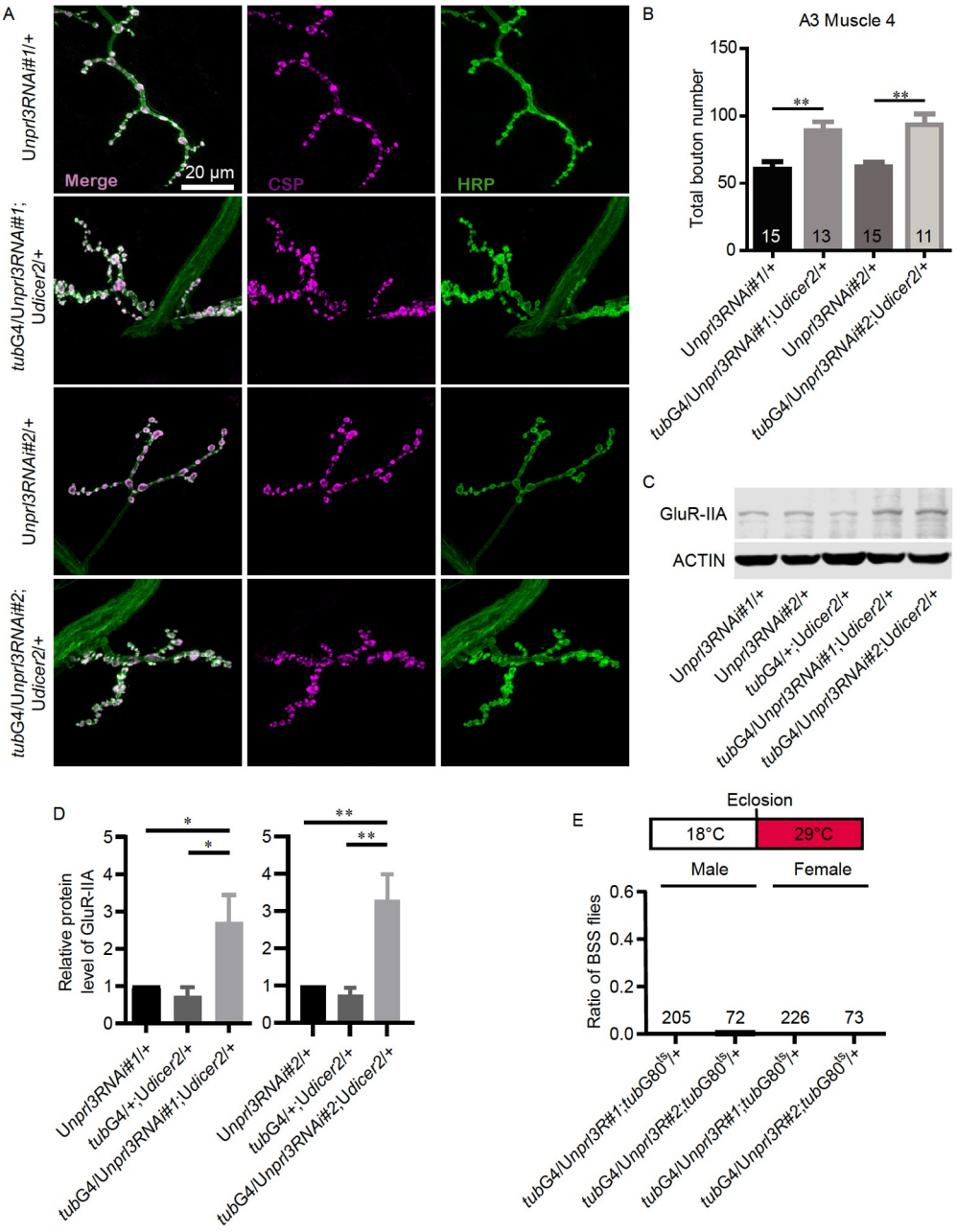

Figure 6 Knocking down *nprl3* led to an increased number of synaptic boutons. A, Representative immunostaining images of NMJ boutons in A3 Muscle 4 of *nprl3* RNAi groups (*tub*GAL4/UAS*nprl3*RNAi1;UAS*dicer2*/+, *tub*GAL4/UAS*nprl3*RNAi2;UAS*dicer2*/+) and control groups (UAS*nprl3*RNAi1/+, UAS*nprl3*RNAi2/+). Horse radish peroxidase (HRP) and cysteine string proteins (CSP) are both presynaptic markers. B, The total count of bouton number of A3 M4. The number of flies used is indicated on the bar. C, Representative Western blot analysis of GluR-IIA in adult flies of the indicated genotypes. D, Quantification of the GluR-IIA to ACTIN ratio in (C), which was normalized to the value obtained for UAS*nprl3*RNAi. n=4. E, Knocking down *nprl3* in the adult stage by *tub*GAL80^{ts} did not induce bang-sensitive seizure behavior in male or female flies. The number of flies used is indicated on the graph. Statistical significance (*, P<0.05; **, P<0.01) was calculated using one-way ANOVA with Bonferroni multiple-comparison test.

verity of the damaging effect of *NPRL3* mutations. Moreover, brain somatic mutations were identified in DEPDC5-associated epilepsy, which may also help explain the severity of the phenotypes (Liu et al., 2020). Somatic mutations can influence the occurrence and development of epilepsy, which contributes to phenotypic heterogeneity (Bedrosian et al., 2022; Chung et al., 2023). However, since brain samples are not available in this study, we are not able to further explore the possibility of mosaic mutations. Furthermore, incomplete penetrance existed in family 1, as four asymptomatic carriers (IV:7, IV:11, V:2 and V:7) were identified (Figure 1A). However, non-symptomatic carriers may have subtle abnormalities that are very difficult to detect by neuroimaging (Sone, 2021). In addition, seizure susceptibility is influenced by genetic backgrounds such as genetic modifications, bi-allelic mutation, second-hit mosaic mutation, and environ-

mental factors including living environment and stress. All or some of these factors could contribute to the differences in phenotypes (Hauser et al., 2018; Jones et al., 2014; Liu et al., 2020; McTague et al., 2016; Ribierre et al., 2018). In our study, although these mutation carriers (IV:7, IV:11, V:2 and V:7 in family 1) displayed no clinical symptoms, it is not clear whether these individuals will develop epilepsy in the future. Thus, long-term follow-up studies of these individuals are warranted.

The *NPRL3* mutations identified in our study sustained a comparable or higher protein expression level relative to WT, but the mutant NPRL3 proteins did not appear to function normally. NPRL2 and NPRL3 dimerize to carry out the GAP activity of GATOR1, while the INT and CTD domains of NPRL3 are considered to be important for its binding to NPRL2 (Shen et al., 2018). Here, we showed for the first time that each domain of NPRL3 interacted with NPRL2, and the mutations we identified in the families did not affect binding affinities to NPRL2, including the severely truncated NPRL3 p.Ile107Profs*56 (Figure 3A–I). This implies that NPRL3 mutants can still bind to NPRL2 through the remaining domains. The crystal structure of GATOR1 indicates that there may be multidomain interactions between NPRL3 and NPRL2 (Shen et al., 2018), which is consistent with our co-IP results (Figure 3C). Moreover, we found that *NPRL3* mutations abolished the interaction with DEPDC5 (Figure 3F). It is possible that NPRL3 directly binds with DEPDC5, and the mutations disrupt this binding. Alternatively, *NPRL3* mutations may alter the conformation of the NPRL3/NPRL2 dimer and thus affect the binding between DEPDC5 and this dimer. Overall, the *NPRL3* mutants lose the ability to integrate into and form functional GATOR1 complexes.

Leucine can activate the mTOR pathway through the well-studied SAR1B/sestrin2-GATOR2-GATOR1-Rag GTPase cascade (Chen et al., 2021; Wolfson et al., 2016). Here, leucine acts as an agonist to induce activation of mTORC1. Under this activated state, the *NPRL3* mutations further increased the activation level of mTORC1 signaling, likely due to impaired inhibitory activities of GATOR1 (Figure 4). However, we did not observe an obvious effect of NPRL3-WT on mTORC1 signaling compared with the vector control. This may be a result of the "ceiling effect", as endogenously expressed NPRL3 in these cells may suppress mTORC1 signaling at maximum capacity. Mutant NPRL3, on the other hand, may compete with WT endogenous NPRL3 proteins in the formation of the GATOR1 complex, thus leading to elevated activation of mTORC1 signaling. These findings also support the notion that NPRL3 mutants are functionally defective in regulating cellular signaling.

Germline knockout of any one of the GATOR1 components in mice is embryonic lethal, while heterozygous knockouts that have been characterized do not exhibit seizure phenotypes (Dutchak et al., 2015; Hughes et al., 2017; Kowalczyk et al., 2012). A recent study reported the occurrence of spontaneous seizures in mice with *Nprl3*, *Nprl2* or *Depdc5* knockout in the telencephalon, demonstrating a causal relationship between GATOR1 deficit and seizure events (Ishida et al., 2022). Here, we confirmed these findings in flies, indicating an evolutionary conservation of the function of GATOR1 components. Epilepsy-like behaviors were increased in flies with *nprl3*, *nprl2* or *iml1* knockdown in all cells of the body (Figure 5A–D), which is more similar to human mutation carriers (who are defective for these components throughout the body) than to conditional knockout mice (Ishida et al., 2022). The KD efficiency was not the highest for *iml1*, although the behavioral phenotypes of the *iml1* RNAi flies were the most severe (Figures S9 and S11 in Supporting Information). We also observed the lowest survival rates for *iml1* RNAi flies, and very few adult *iml1* RNAi flies could be collected for experiments. This is consistent with the severity of the epilepsy-like phenotype. In line with these results, it has been reported that *nprl2* and *nprl3* mutant flies eclose at a substantially reduced rate, while no *iml1* mutants eclose (Wei et al., 2016). Among the three components of the GATOR1 complex, DEPDC5 directly binds to Rag GTPase (RAGA) through its critical strip to exert a strong inhibitory action, and the absence of DEPDC5 substantially reduces the binding affinity of Rag GTPases with NPRL2-NPRL3 (Shen et al., 2018). Overall, we suspect that the reason *iml1* RNAi flies showed the most severe seizure phenotype is due to the more critical role of IML1/DEPDC5 played in the GATOR1 complex.

Global knockdown of *nprl3* led to significant overgrowth of the synaptic terminal at the NMJ (Figure 6A and B). Synapse turnover is a highly dynamic and regulated process (Grinnell, 1995). The increased bouton number in *nprl3* RNAi flies indicates that *nprl3* acts to inhibit bouton formation and/or promote bouton elimination at the NMJ. Consistent with the fact that the neurotransmitter contained in type I boutons is mainly the excitatory neurotransmitter glutamate, we observed increased glutamate receptor levels in these flies, suggesting that *nprl3* deficiency could lead to excitation-inhibition (E-I) imbalance, which is believed to be a major cause of seizures (Staley, 2015). These morphological alterations at larval NMJs demonstrate developmental defects in these flies, which may contribute to epilepsy-like behaviors in adults. To validate this, we first attempted to knock down *nprl3* specifically during development using the *tub*G80^{ts} system. Unfortunately, these flies did not survive to adulthood, possibly due to a combination of *nprl3* deficiency and high temperature during development (29°C). Knocking down *nprl3* specifically in adults did not enhance epilepsy-like behavior, strongly suggesting that a lack of *nprl3* during development is necessary for the epilepsy-like phenotype.

In conclusion, we identified three novel *NPRL3* mutations

in three families with focal epilepsy, which expanded the genotypic spectrum of *NPRL3* variants. The mutations impaired the interaction between NPRL3 and DEPDC5 and resulted in increased activation of the mTORC1 pathway (Figure S13 in Supporting Information). Moreover, we found that knocking down one of the three GATOR1 components increased epilepsy-like behavior in flies and demonstrated a role of *nprl3* in synaptic development, further supporting the notion that deficits in GATOR1 signaling contribute to the pathogenesis of epilepsy.

MATERIALS AND METHODS

Families and patients

Three Chinese families with autosomal dominant focal epilepsy were identified at Xiangya Hospital (Changsha, China). Informed consent was obtained from all the participants, and study protocols were approved by the Ethics Committee of Huazhong University of Science and Technology according to the Declaration of Helsinki. For genetic testing, genomic DNA was extracted from peripheral blood samples as previously reported (Liu et al., 2008).

Genotyping and linkage analysis

Linkage analysis was performed in 17 members in family 1, and more than 870,000 SNP markers were subjected to genotyping using the Infinium OmniZhongHua-8 v1.3 BeadChip (Illumina, USA). Multipoint LOD scores were calculated using Merlin and performed by assuming the family as an autosomal dominant pattern of inheritance with a disease allele frequency of 0.0001 and a penetrance value of 0.8. Multiplex PCR with fluorescently labeled primers was used to amplify markers (Table S6 in Supporting Information), and PCR products were analyzed by capillary electrophoresis.

Whole exome sequencing

Genomic DNA samples from patients in family I (III:6, III:12 and V:6) and family II (III:4 and IV:6), as well as individuals in family III (I:1, I:2 and II:1), were sent to an external core facility (WuXi NextCode Genomics (Shanghai) Co., Ltd., China) for exome sequencing using the Illumina HiSeq 2500 platform with 100-bp paired reads. The mean depth of base mapped to the target region was ≥92.84×, and the coverage of sequencing depth was ≥94.22% sequenced at 20× and higher. The candidate variants were filtered with an allele frequency greater than 0.001 in public databases (1000Genome, dbSNP, ExAC and gnomAD database). Then heterozygous variants, nonsynonymous variants, and likely loss-of-function variants (i.e., nonsense, frameshift, indel and splicing) were retained for further analysis. The conservation and functional effects of the variants were predicted using *in silico* analysis tools PolyPhen-2, PROVEAN, SIFT, and Mutation Taster.

Mutation analysis

To analyze the breakpoint junctions of the microdeletion in the *NPRL3* gene in family 1, primers were designed at the apparent boundaries, RT-qPCR was carried out to narrow down to a possible range, and then the long-range PCR product was subjected to Sanger sequencing. To validate the microdeletion at the mRNA level, total RNA was extracted from PBLs from family members, and reverse transcription was carried out to synthesize cDNA. The mRNA level of *NPRL3* was analyzed by qPCR and normalized to *HBB*, a reference gene. Fold differences were calculated using the $2^{-\Delta\Delta Ct}$ method.

The exons of *NPRL3* were amplified and then subjected to Sanger sequencing to confirm whether the variant co-segregated with the disease in the families. The DNA fragment containing the *NdeI* restriction enzyme site was created by PCR, and analysis was performed to determine whether the mutation in family 2 was absent in 100 unrelated normal controls. The DNA fragment of *NARFL* containing the *KpnI* restriction enzyme site was created by PCR, and analysis was performed to determine whether the mutation co-segregated with the disease in family 2. The primers used are listed in Table S7 in Supporting Information.

Cell culture and transfection

COS7, HEK293T, and HEK293 cells were cultured in antibiotic-free Dulbecco's modified Eagle's medium (Gibco, USA) with 10% (v/v) fetal bovine serum (FBS, Gibco) and transfected with WT or mutant NPRL3 plasmids using PolyJet™ reagent (SignaGen, USA). PBLs were cultured in RPMI-1640 medium (Gibco) supplemented with 10% FBS.

Cell treatment

The starvation experiments were conducted as previously reported (Dawson et al., 2020). HEK293 cells were washed twice with handmade Earle's balanced salt solution (EBSS) and cultured with EBSS for another 24 h post-transfection.

For leucine restimulation treatments after starvation, the cells were stimulated for the indicated duration (0, 10, 20, 30, 40, 50 and 60 min) by directly adding high concentration leucine stock solution at the indicated concentrations (0, 10, 50, 100, 500 and 1,000 μmol L^{-1}).

For the CHX chase assay, HEK293 cells were treated with 30 μg mL^{-1} CHX (APExBIO, USA) at 24 h after transfection and then harvested at different time points (0, 4, 8 and 12 h). The samples were analyzed by Western blotting. CHX has been

shown to activate mTORC1 activity by increasing the intracellular level of amino acids, and cells were treated with 50 μg mL^{-1} CHX for 45 min as reported (Watanabe-Asano et al., 2014).

Plasmid construction

Full-length *NPRL3* and *NPRL2* cDNA were amplified from a cDNA library generated using HEK293 cells. The full-length *NPRL3* cDNA was then cloned into the p3×FLAG-(DYKDDDDK tag)-MYC-CMV24 and pEGFP-C1 vectors. The full-length *NPRL2* cDNA sequence was cloned into the pEGFP-N1 and pcDNA3.1(+) vectors. Mutant *NPRL3* plasmids were generated based on the WT-*NPRL3* plasmid using site-directed mutagenesis. The domains of the *NPRL3* gene were cloned into the pEGFP-C1 vector based on the WT-*NPRL3* plasmid. All constructed plasmids were verified by Sanger sequencing. The primers used are listed in Table S8 in Supporting Information.

Fly strains

Flies were maintained on standard media at 25°C. All strains were obtained from Bloomington Stock Center, Vienna Drosophila Resource Center (VDRC), TsingHua Fly Center (THFC) or as gifts from colleagues. All fly crosses were carried out at 25°C unless noted otherwise. The following fly strains were used in this study: UAS*dicer2* (BDSC24650), *tub*GAL4 and *tub*GAL80^{ts} (a gift from Ravi Allada), *actin*-GAL4 (a gift from Prof Liming Wang), Trip (THFC and Bloomington control strain), KK and GD (VDRC control strain), UAS*nprl3*RNAi#1 (TH03133.N), UAS*nprl3*RNAi#2 (BL55384), UAS*nprl2*RNAi#1 (TH03825.N) and UAS*nprl2*RNAi#2 (BL57538), UAS*iml1*RNAi#1 (V110386) and UAS*iml1*RNAi#2 (V16390).

Analysis of mRNA expression

RT-qPCR was performed to analyze the mRNA levels of *NPRL3* in HEK293 cells transfected with WT and mutant FLAG-NPRL3. Twenty-four hours after transfection, cells were homogenized using TRIzol reagent (Life Technologies, USA). Total RNA was isolated by chloroform and isopropanol, and cDNA was prepared using HifairIII 1st strand cDNA synthesis SuperMix for qPCR (YEASEN Biotechnology, Shanghai, China). The cDNA was then subjected to RT-qPCR, and the primers used are listed in Table S9 in Supporting Information.

Three days after eclosion, 20 male flies from each genotype were collected into centrifuge tubes. Whole flies were homogenized in TRIzol reagent. The RNA extraction procedure followed that in Ref. (Bu et al., 2019). Then, the total RNA was reverse transcribed to cDNA by using TransScript Green One-Step RT-qPCR SuperMix (TransGen Biotechnology, Beijing, China), and the qPCR procedure was carried out by a Step One Plus Real-Time PCR System (Life Technologies). The primers used to assess RNAi efficiency are listed in Table S9 in Supporting Information.

Western blot and co-immunoprecipitation

After transfection, HEK293 cells were washed once with phosphate-buffered saline (PBS) and lysed using cell lysis buffer (P0013, Beyotime, Shanghai, China) supplemented with protease and phosphatase inhibitor cocktails (Roche, Itlay). The supernatant was collected and analyzed by Western blotting. For GluR-IIA immunoblotting, 50 flies were homogenized in 100 μL RIPA buffer, and the supernatant was subjected to SDS-PAGE.

For co-immunoprecipitation experiments, the co-transfected HEK293T cells were washed with cold PBS and lysed on ice. Then, 100 μL of the collected supernatant served as the input, and the remaining sample was divided into two aliquots, which were incubated with FLAG or GFP antibodies or IgG overnight at 4°C. The samples were then incubated with Protein A agarose beads for 4 h. The immunoprecipitates were washed 5 times with lysis buffer and denatured prior to Western blotting.

Immunofluorescence

The transfected HEK293 cells in confocal dishes were fixed in 4% paraformaldehyde for 30 min, washed three times with cold PBS, and then the cells were permeabilized in 0.5% Triton X-100 for 15 min. Cells were subsequently rinsed three times in PBS and blocked with 5% BSA for 30 min. Next, the cells were incubated with anti-FLAG (diluted in 1% BSA) at 4°C overnight and washed three times with PBS. Subsequently, the cells were incubated with fluorescently labeled secondary antibodies, washed with PBS three times, stained with DAPI for 5 min and washed with PBS. The cells were imaged by confocal microscopy.

The NMJs of 3rd instar larvae were dissected as previously described (Brent et al., 2009). HRP-positive boutons of NMJ presynaptic terminals were measured and quantified using ImageJ software. Type I boutons of muscle 4 in A3 NMJs were analyzed using the same standard, and 10 NMJs were analyzed per genotype.

Bang-sensitive seizure assay

A bang-sensitive seizure assay was performed as previously reported (Pavlidis and Tanouye, 1995). Briefly, 100 flies of each genotype were collected with the use of CO_2 at 2–3 days after eclosion, and flies were transferred to vials with fresh media in groups of 10. The flies were assayed 7 days later unless otherwise specified. For behavioral testing, these flies

were gently transferred to empty vials. The vials were mechanically stimulated (bang) with a VWR vortex mixer at maximum speed for 10 s. The number of flies experiencing seizure- and paralysis-like behaviors in response to the bang was measured based on video recording, and the recovery time for each fly was also measured. Care was taken to minimize shaking and vibrations of the vials before testing.

Reagents and antibodies

The primary and secondary antibodies used are as follows: anti-DDDDK tag (MBL, USA, 1:4,000), anti-β-actin (ABclonal, Wuhan, China, 1:3,000), anti-GAPDH (ABclonal, 1:3,000), rabbit anti-phospho-RPS6-S240/244 (ABclonal, 1:1,000), rabbit anti-RPS6 (ABclonal, 1:1,000), anti-p70 S6 kinase (Cell Signaling Technology, USA, 1:1,000), anti-phospho-*Drosophila* p70 S6 kinase (Thr398) (Cell Signaling Technology, 1:1,000), anti-DEPDC5 (Abcam, USA, 1:1,000), anti-GFP (ABclonal, 1:3,000), mouse IgG (ProteinTech, USA, 1 mg mL^{-1}), rabbit IgG (ProteinTech), HRP goat anti-mouse IgG (H+L) (ABclonal, 1:10,000), HRP goat anti-rabbit IgG (H+L) (ABclonal, 1:10,000), Alexa Fluor 488 labeled goat anti-rabbit IgG (Life Technologies, 1:1,000), Alexa Fluor 594 labeled goat anti-mouse IgG (Life Technologies, 1:1,000), anti-mouse CSP (DSHB, 1:100), 488-phalloidine conjugates (ProteinTech, 1:50), anti-HRP-TRITC (Jackson ImmunoResearch Laboratories, USA, 1:200), anti-mouse Cy5 (Abcam, 1:200), anti-mouse GluR-IIA (Developmental Studies Hybridoma Bank, USA, 1:1,000), and anti-rabbit ACTIN (ABclonal, 1:1,000).

Statistical analysis

Comparisons between two groups were conducted by unpaired two-tailed Student's *t*-test for parametric data, and comparisons between multiple groups were conducted by one-way ANOVA. Differences with P values<0.05 were considered significant.

Compliance and ethics *The author(s) declare that they have no conflict of interest.*

Acknowledgements *This work was supported by the National Natural Science Foundation of China (32270663, 31871262, U20A20355, 32022035), Shanghai Municipal Science and Technology Major Project (2018SHZDZX05), and the Ministry of Science and Technology of China STI 2030-Major Projects (2021ZD0203202). We would like to thank all the participants in this study. We would also like to thank the Tsinghua Fly Center for providing fly stocks.*

References

Baldassari, S., Picard, F., Verbeek, N.E., van Kempen, M., Brilstra, E.H., Lesca, G., Conti, V., Guerrini, R., Bisulli, F., Licchetta, L., et al. (2019). The landscape of epilepsy-related GATOR1 variants. Genet Med 21, 398–408.

Bar-Peled, L., Chantranupong, L., Cherniack, A.D., Chen, W.W., Ottina, K. A., Grabiner, B.C., Spear, E.D., Carter, S.L., Meyerson, M., and Sabatini, D.M. (2013). A tumor suppressor complex with GAP activity for the Rag GTPases that signal amino acid sufficiency to mTORC1. Science 340, 1100–1106.

Bedrosian, T.A., Miller, K.E., Grischow, O.E., Schieffer, K.M., LaHaye, S., Yoon, H., Miller, A.R., Navarro, J., Westfall, J., Leraas, K., et al. (2022). Detection of brain somatic variation in epilepsy-associated developmental lesions. Epilepsia 63, 1981–1997.

Brent, J.R., Werner, K.M., and McCabe, B.D. (2009). *Drosophila* larval NMJ dissection. J Vis Exp 24, e1107.

Bu, B., He, W., Song, L., and Zhang, L. (2019). Nuclear envelope protein MAN1 regulates the *Drosophila* circadian clock via period. Neurosci Bull 35, 969–978.

Canavati, C., Klein, K.M., Afawi, Z., Pendziwiat, M., Abu Rayyan, A., Kamal, L., Zahdeh, F., Qaysia, I., Helbig, I., and Kanaan, M. (2019). Inclusion of hemimegalencephaly into the phenotypic spectrum of NPRL3 pathogenic variants in familial focal epilepsy with variable foci. Epilepsia 60, e67–e73.

Chen, J., Ou, Y., Luo, R., Wang, J., Wang, D., Guan, J., Li, Y., Xia, P., Chen, P.R., and Liu, Y. (2021). SAR1B senses leucine levels to regulate mTORC1 signalling. Nature 596, 281–284.

Chung, C., Yang, X., Bae, T., Vong, K.I., Mittal, S., Donkels, C., Westley Phillips, H., Li, Z., Marsh, A.P.L., Breuss, M.W., et al. (2023). Comprehensive multi-omic profiling of somatic mutations in malformations of cortical development. Nat Genet 55, 209–220.

Crompton, D.E., Scheffer, I.E., Taylor, I., Cook, M.J., McKelvie, P.A., Vears, D.F., Lawrence, K.M., McMahon, J.M., Grinton, B.E., McIntosh, A.M., et al. (2010). Familial mesial temporal lobe epilepsy: a benign epilepsy syndrome showing complex inheritance. Brain 133, 3221–3231.

Dawson, R.E., Nieto Guil, A.F., Robertson, L.J., Piltz, S.G., Hughes, J.N., and Thomas, P.Q. (2020). Functional screening of GATOR1 complex variants reveals a role for mTORC1 deregulation in FCD and focal epilepsy. Neurobiol Dis 134, 104640.

Devinsky, O., Vezzani, A., O'Brien, T.J., Jette, N., Scheffer, I.E., de Curtis, M., and Perucca, P. (2018). Epilepsy. Nat Rev Dis Primers 4, 18024.

Dibbens, L.M., de Vries, B., Donatello, S., Heron, S.E., Hodgson, B.L., Chintawar, S., Crompton, D.E., Hughes, J.N., Bellows, S.T., Klein, K. M., et al. (2013). Mutations in DEPDC5 cause familial focal epilepsy with variable foci. Nat Genet 45, 546–551.

Dutchak, P.A., Laxman, S., Estill, S.J., Wang, C., Wang, Y., Wang, Y., Bulut, G.B., Gao, J., Huang, L.J., and Tu, B.P. (2015). Regulation of hematopoiesis and methionine homeostasis by mTORC1 Inhibitor NPRL2. Cell Rep 12, 371–379.

Fridell, Y.W.C., Sánchez-Blanco, A., Silvia, B.A., and Helfand, S.L. (2005). Targeted expression of the human uncoupling protein 2 (hUCP2) to adult neurons extends life span in the fly. Cell Metab 1, 145–152.

Grinnell, A.D. (1995). Dynamics of nerve-muscle interaction in developing and mature neuromuscular junctions. Physiol Rev 75, 789–834.

Hauser, R.M., Henshall, D.C., and Lubin, F.D. (2018). The epigenetics of epilepsy and its progression. Neuroscientist 24, 186–200.

Hughes, J., Dawson, R., Tea, M., McAninch, D., Piltz, S., Jackson, D., Stewart, L., Ricos, M.G., Dibbens, L.M., Harvey, N.L., et al. (2017). Knockout of the epilepsy gene Depdc5 in mice causes severe embryonic dysmorphology with hyperactivity of mTORC1 signalling. Sci Rep 7, 12618.

Ishida, S., Zhao, D., Sawada, Y., Hiraoka, Y., Mashimo, T., and Tanaka, K. (2022). Dorsal telencephalon-specific *Nprl2*- and *Nprl3*-knockout mice: novel mouse models for GATORopathy. Hum Mol Genet 31, 1519–1530.

Ji, Y., and Clark, D.V. (2006). The purine synthesis gene *Prat2* is required for *Drosophila* metamorphosis, as revealed by inverted-repeat-mediated RNA interference. Genetics 172, 1621–1631.

Jones, N.C., O'Brien, T.J., and Carmant, L. (2014). Interaction between sex and early-life stress: Influence on epileptogenesis and epilepsy

comorbidities. Neurobiol Dis 72, 233–241.
Keshishian, H., Broadie, K., Chiba, A., and Bate, M. (1996). The *Drosophila* neuromuscular junction: a model system for studying synaptic development and function. Annu Rev Neurosci 19, 545–575.
Kingdom, R., and Wright, C.F. (2022). Incomplete penetrance and variable expressivity: from clinical studies to population cohorts. Front Genet 13, 920390.
Korenke, G.C., Eggert, M., Thiele, H., Nürnberg, P., Sander, T., and Steinlein, O.K. (2016). Nocturnal frontal lobe epilepsy caused by a mutation in the GATOR1 complex gene *NPRL3*. Epilepsia 57, e60–e63.
Kowalczyk, M.S., Hughes, J.R., Babbs, C., Sanchez-Pulido, L., Szumska, D., Sharpe, J.A., Sloane-Stanley, J.A., Morriss-Kay, G.M., Smoot, L.B., Roberts, A.E., et al. (2012). Nprl3 is required for normal development of the cardiovascular system. Mamm Genome 23, 404–415.
Li, Y., Zhao, X., Wang, S., Xu, K., Zhao, X., Huang, S., and Zhu, S. (2021). A novel loss-of-function mutation in the *NPRL3* gene identified in Chinese familial focal epilepsy with variable foci. Front Genet 12, 766354.
Liu, H., Du, C., Luo, J., Qiu, X., Li, Z., Lou, Q., Yin, Z., and Zheng, F. (2017). A novel mutation in nuclear prelamin a recognition factor-like causes diffuse pulmonary arteriovenous malformations. Oncotarget 8, 2708–2718.
Liu, J.Y., Dai, X., Sheng, J., Cui, X., Wang, X., Jiang, X., Tu, X., Tang, Z., Bai, Y., Liu, M., et al. (2008). Identification and functional characterization of a novel splicing mutation in RP gene *PRPF31*. Biochem Biophys Res Commun 367, 420–426.
Liu, L., Chen, Z.R., Xu, H.Q., Liu, D.T., Mao, Y., Liu, H.K., Liu, X.R., Zhou, P., Lin, S.M., Li, B., et al. (2020). *DEPDC5* variants associated malformations of cortical development and focal epilepsy with febrile seizure plus/febrile seizures: the role of molecular sub-regional effect. Front Neurosci 14, 821.
Liu, Y., Tian, X., Ke, P., Gu, J., Ma, Y., Guo, Y., Xu, X., Chen, Y., Yang, M., Wang, X., et al. (2022). KIF17 modulates epileptic seizures and membrane expression of the NMDA receptor subunit NR2B. Neurosci Bull 38, 841–856.
McGuire, S.E., Mao, Z., and Davis, R.L. (2004). Spatiotemporal gene expression targeting with the TARGET and Gene-Switch systems in *Drosophila*. Sci STKE 2004(220), pl6.
McTague, A., Howell, K.B., Cross, J.H., Kurian, M.A., and Scheffer, I.E. (2016). The genetic landscape of the epileptic encephalopathies of infancy and childhood. Lancet Neurol 15, 304–316.
Menon, K.P., Carrillo, R.A., and Zinn, K. (2013). Development and plasticity of the *Drosophila* larval neuromuscular junction. WIREs Dev Biol 2, 647–670.
Myers, C.T., and Mefford, H.C. (2015). Advancing epilepsy genetics in the genomic era. Genome Med 7, 91.
Neklesa, T.K., and Davis, R.W. (2009). A genome-wide screen for regulators of TORC1 in response to amino acid starvation reveals a conserved Npr2/3 complex. PLoS Genet 5, e1000515.
Pavlidis, P., and Tanouye, M.A. (1995). Seizures and failures in the giant fiber pathway of *Drosophila* bang-sensitive paralytic mutants. J Neurosci 15, 5810–5819.
Perucca, P. (2018). Genetics of focal epilepsies: what do we know and where are we heading? Epilepsy Curr 18, 356–362.
Ribierre, T., Deleuze, C., Bacq, A., Baldassari, S., Marsan, E., Chipaux, M., Muraca, G., Roussel, D., Navarro, V., Leguern, E., et al. (2018). Second-hit mosaic mutation in mTORC1 repressor DEPDC5 causes focal cortical dysplasia-associated epilepsy. J Clin Invest 128, 2452–2458.
Ricos, M.G., Hodgson, B.L., Pippucci, T., Saidin, A., Ong, Y.S., Heron, S. E., Licchetta, L., Bisulli, F., Bayly, M.A., Hughes, J., et al. (2016). Mutations in the mammalian target of rapamycin pathway regulators *NPRL2* and *NPRL3* cause focal epilepsy. Ann Neurol 79, 120–131.
Riney, K., Bogacz, A., Somerville, E., Hirsch, E., Nabbout, R., Scheffer, I. E., Zuberi, S.M., Alsaadi, T., Jain, S., French, J., et al. (2022). International League Against Epilepsy classification and definition of epilepsy syndromes with onset at a variable age: position statement by the ILAE Task Force on Nosology and Definitions. Epilepsia 63, 1443–1474.
Saxton, R.A., and Sabatini, D.M. (2017). mTOR signaling in growth, metabolism, and disease. Cell 168, 960–976.
Scheffer, I.E., Bhatia, K.P., Lopes-Cendes, I., Fish, D.R., Marsden, C.D., Andermann, E., Andermann, F., Desbiens, R., Keene, D., Cendes, F., et al. (1995). Autosomal dominant nocturnal frontal lobe epilepsy. Brain 118, 61–73.
Scheffer, I.E., Phillips, H.A., O'Brien, C.E., Saling, M.M., Wrennall, J.A., Wallace, R.H., Mulley, J.C., and Berkovic, S.F. (1998). Familial partial epilepsy with variable foci: a new partial epilepsy syndrome with suggestion of linkage to chromosome 2. Ann Neurol 44, 890–899.
Schmid, A., Hallermann, S., Kittel, R.J., Khorramshahi, O., Frölich, A.M. J., Quentin, C., Rasse, T.M., Mertel, S., Heckmann, M., and Sigrist, S.J. (2008). Activity-dependent site-specific changes of glutamate receptor composition *in vivo*. Nat Neurosci 11, 659–666.
Shen, K., Huang, R.K., Brignole, E.J., Condon, K.J., Valenstein, M.L., Chantranupong, L., Bomaliyamu, A., Choe, A., Hong, C., Yu, Z., et al. (2018). Architecture of the human GATOR1 and GATOR1-Rag GTPases complexes. Nature 556, 64–69.
Sim, J.C., Scerri, T., Fanjul-Fernández, M., Riseley, J.R., Gillies, G., Pope, K., van Roozendaal, H., Heng, J.I., Mandelstam, S.A., McGillivray, G., et al. (2016). Familial cortical dysplasia caused by mutation in the mammalian target of rapamycin regulator *NPRL3*. Ann Neurol 79, 132–137.
Sone, D. (2021). Making the invisible visible: advanced neuroimaging techniques in focal epilepsy. Front Neurosci 15, 699176.
Staley, K. (2015). Molecular mechanisms of epilepsy. Nat Neurosci 18, 367–372.
Tang, B., Li, B., Gao, L.D., He, N., Liu, X.R., Long, Y.S., Zeng, Y., Yi, Y. H., Su, T., and Liao, W.P. (2020). Optimization of *in silico* tools for predicting genetic variants: individualizing for genes with molecular sub-regional stratification. Brief Bioinform 21, 1776–1786.
Wang, J., Lin, Z.J., Liu, L., Xu, H.Q., Shi, Y.W., Yi, Y.H., He, N., and Liao, W.P. (2017). Epilepsy-associated genes. Seizure 44, 11–20.
Watanabe-Asano, T., Kuma, A., and Mizushima, N. (2014). Cycloheximide inhibits starvation-induced autophagy through mTORC1 activation. Biochem Biophys Res Commun 445, 334–339.
Weckhuysen, S., Marsan, E., Lambrecq, V., Marchal, C., Morin-Brureau, M., An-Gourfinkel, I., Baulac, M., Fohlen, M., Kallay Zetchi, C., Seeck, M., et al. (2016). Involvement of GATOR complex genes in familial focal epilepsies and focal cortical dysplasia. Epilepsia 57, 994–1003.
Wei, Y., Reveal, B., Cai, W., and Lilly, M.A. (2016). The GATOR1 complex regulates metabolic homeostasis and the response to nutrient stress in *Drosophila melanogaster*. G3 6, 3859–3867.
Wolfson, R.L., Chantranupong, L., Saxton, R.A., Shen, K., Scaria, S.M., Cantor, J.R., and Sabatini, D.M. (2016). Sestrin2 is a leucine sensor for the mTORC1 pathway. Science 351, 43–48.
Wullschleger, S., Loewith, R., and Hall, M.N. (2006). TOR signaling in growth and metabolism. Cell 124, 471–484.

SUPPORTING INFORMATION

The supporting information is available online at https://doi.org/10.1007/s11427-022-2313-1. The supporting materials are published as submitted, without typesetting or editing. The responsibility for scientific accuracy and content remains entirely with the authors.